Isosorbide dimethyl ether enables interfacial regulation to boost the aqueous zinc-sulfur battery performance

Shan Wang,[†,a] Shuaiqi Wang,[†,a] Xueqi Guo,[a] Wenhao Xu,[a] Linghao Su,[a] Lanju Sun,[a,b,*] Hao Wu,[b,*] Jie Wang[a,*]

[a] Qingdao Engineering Research Center of Agricultural Recycling Economy Materials, College of Chemistry and Pharmaceutical Sciences, Qingdao Agricultural University, 266109 Qingdao, China.

[b] Institute of Frontier Chemistry, School of Chemistry and Chemical Engineering, Shandong University, 266237 Qingdao, China.

EXPERIMENTAL PROCEDURES

Materials: The reagents used in this work include sulfur powder (S, Sinopharm Chemical Reagent Co, Ltd, China), Isosorbide dimethyl ether (ID, $C_8H_{14}O_4$, Macklin, China), zinc trifluoromethanesulfonate ($Zn(OTf)_2$, Macklin, China), Iodine (I_2, Macklin, China), polyvinylidene fluoride (PVDF), carbon black, and carbon nanotubes (CNTs). All reagents were of analytical grade and were used as received without further purification.

Electrolyte preparation: 2 M $Zn(OTf)_2$ + ID + I_2 + water, denoted as IDW, was prepared by first mixing ID and water at a volume ratio of 2:3. $Zn(OTf)_2$ salt was then added dropwise to the mixture under continuous stirring to achieve a final concentration of 2 M. I_2 was introduced as an additive, accounting for 0.15 wt% of the total electrolyte mass.

For comparison, control electrolytes were also prepared similarly: 2 M $Zn(OTf)_2$ + I_2 + H_2O (without ID, W), Additionally, IDW electrolytes with varying ID volume concentrations were also prepared to evaluate the effect of ID concentration on electrochemical performance and safety.

Fabrication of S@CNTs material: Sulfur powder and CNTs were mixed at a mass ratio of 1:1 and ground thoroughly for 30 minutes. The mixture was then heated at 155 °C for 16 hours under a nitrogen atmosphere.

Physical characterization: The microstructure of the samples was characterized using transmission electron microscope (TEM, JSM) equipped with energy dispersive X-ray spectrometer (EDS). Raman spectra were recorded using a Raman microscope (Renishaw plc, inVia Reflex) equipped with a 532 nm laser excitation source. X-ray diffraction (XRD) patterns were obtained using a Bruker D8 ADVANCE diffractometer with Cu Kα radiation to analyze the crystalline structure of the samples. The sulfur content was quantified using a sulfur-carbon analyzer (S-C analyzer HIR 944). X-ray photoelectron spectroscopy (XPS, Thermo Scientific K-Alpha) was employed to investigate the chemical composition and oxidation states of the elements present. The specific surface area was determined via nitrogen adsorption–desorption isotherms using the BET method. Organic functional groups in the samples were analyzed by Fourier-transform infrared spectroscopy (FTIR, SHIMADZU IR Spirit-T). Furthermore, the chemical interaction between ID and I_2 was studied using ^{1}H-Nuclear Magnetic Resonance Spectroscopy spectroscopy (AVANCE III HD 400 MHz), with D_2O employed as the deuterated solvent. Contact angle measurements were conducted

via an Optical Contact Angle Meter (OCA20, Germany). Specifically, A 3 μL droplet was released onto the electrode surface using a syringe, and its contact angle was measured by capturing an image with the attached camera, ensuring the droplet remained static for 3 s after image capture.

Electrochemical measurements: CR2032-type coin cells and Zn||Zn symmetric cells were assembled to evaluate the electrochemical performance. The sulfur cathode was prepared by mixing CNT@S with carbon black (10 wt.%) and polyvinylidene fluoride (PVDF, 10 wt%) in N-methyl-2-pyrrolidone (NMP) to form a homogeneous slurry. This slurry was then evenly coated onto carbon cloth substrates (14 mm in diameter) and dried to obtain cathodes with a sulfur loading of 1.5 mg cm^{-2}. In CR2032 coin cells, a 0.02 mm thick zinc sheet served as the anode, and a glass fiber membrane was used as the separator. The electrolytes tested included IDW and W All cells were left to rest for 6 hours prior to electrochemical testing to ensure adequate electrolyte infiltration.

Sulfur loading mass at the cathode: The total sulfur mass loaded on the cathode was measured to be 2.3 mg by averaging three cathode plates. The cathode current collector had a diameter of 14 mm, corresponding to a geometric area of 1.53 cm^2. Based on these values, the areal sulfur loading was calculated to be 1.5 mg cm^{-2}.

The electrolyte dosage was 40 μL, yielding an E/S ratio (electrolyte-to-sulfur ratio) of 40 / 2.3 = 17.4 μL mg^{-1}.

The N/P ratio is defined as the areal capacity of the anode divided by the areal capacity of the cathode. The calculation of the theoretical areal capacity of the anode: A Zn foil with a thickness of 20 μm was employed in this work. Given the theoretical specific capacity of Zn is 820.0 mAh g^{-1} and the density of Zn is 7.14 g cm^{-3}, the theoretical volumetric capacity is calculated as 5850 mAh cm^{-3}. The resulting areal capacity is therefore: 0.002 cm × 5850 mAh cm^{-3} ≈ 11.7 mAh cm^{-2}. With the known areal capacity of the cathode being 2.37 mAh cm^{-2} for IDW-based AZSB and 1.68 mAh cm^{-2} for W-based AZSB, the corresponding N/P ratios are calculated to be 4.93 and 6.96, respectively.

The corresponding data can be found in Table S1.

All electrochemical measurements were conducted with the electrolytes maintained at a constant temperature of 25 °C. Electrochemical characterization was carried out at room temperature using a LAND battery test system (CT2001A, Wuhan Lander Electronics Co., Ltd.) and an electrochemical workstation (CHI760E, CH instrument). Galvanostatic charge–discharge (GCD)

measurements were performed within a voltage window of 0.05–1.60 V vs. Zn^{2+}/Zn; Linear scanning voltammetry (LSV) was conducted within the potential range of 0 V to -0.20 V; Chronoamperometry tests were carried out under a constant overpotential of −150 mV; Cyclic voltammetry (CV) scans were performed between 0.05 V and 1.60 V vs. Zn^{2+}/Zn; Tafel polarization curves were recorded in the potential range of −0.20 V to 0.20 V; Electrochemical impedance spectroscopy (EIS) measurements were conducted at the open-circuit potential (OCP) or at specific charge/discharge voltages (*in-situ* EIS), with a frequency range of 100,000 Hz to 0.01 Hz. Each test of the AZSB was repeated three times to ensure the reliability of the work.

$$j = j_0\left\{exp\left[\frac{\alpha_a zF\eta}{RT}\right] - exp\left[\frac{\alpha_c zF\eta}{RT}\right]\right\} \quad (1)$$

This is a fundamental equation describing the kinetics of electrode reactions, which quantitatively reveals the relationship between the electrode reaction rate (i.e., current density) and the electrode potential[1].

$$r = \frac{2V_m\gamma_{NE}}{zF\eta} \quad (2)$$

The classical nucleation theory is a classic model that describes the initial formation (i.e., nucleation) process of new phases (such as droplets, crystals, and bubbles) in old phases. Its core lies in analyzing the competitive relationship between the reduction of volumetric free energy and the increase of surface free energy when a small nuclear embryo is formed[2].

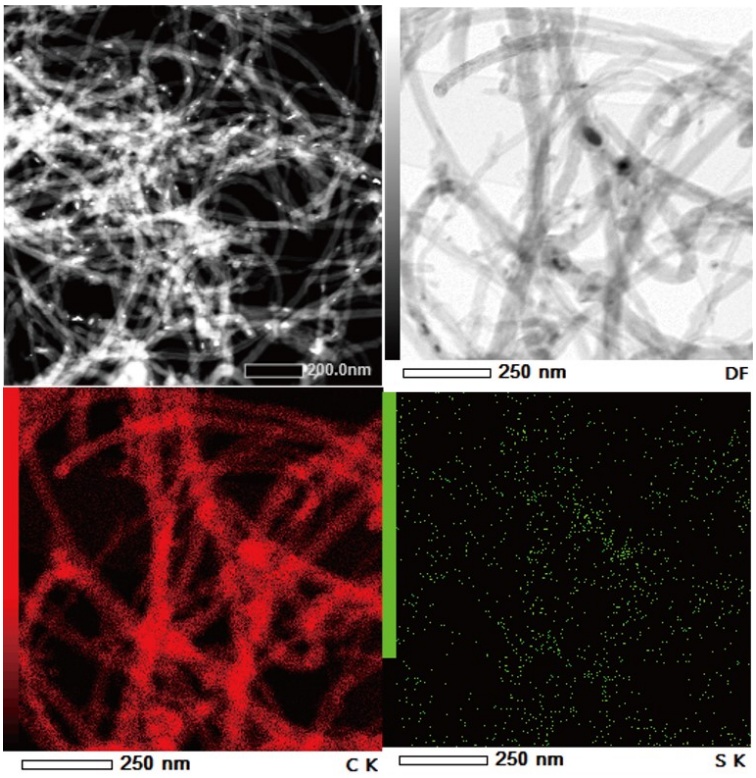

Fig. S1 Dark-field STEM image and bright field STEM images of S@CNT and corresponding elemental distribution maps of S, C and the overlay of S and C.

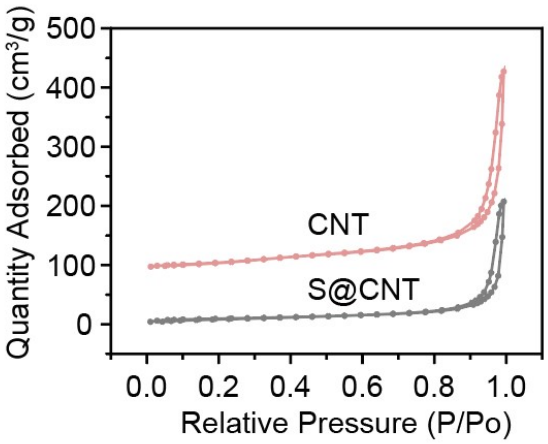

Fig. S2 Nitrogen adsorption and desorption isothermal of CNT and S@CNT.

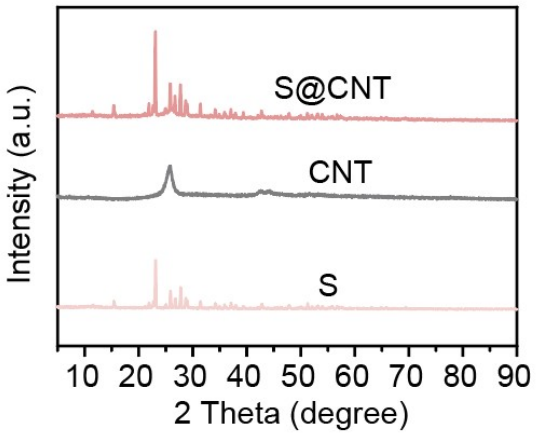

Fig. S3 XRD patterns of S, CNT and S@CNT.

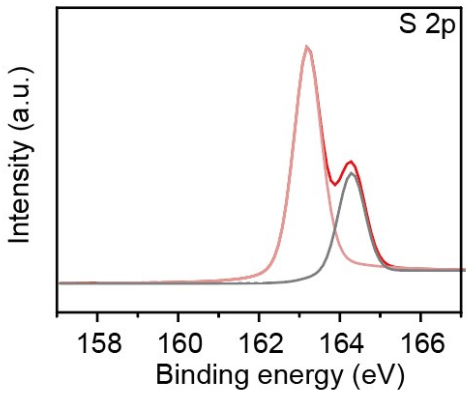

Fig. S4 High-resolution S 2p XPS spectra of S@CNT

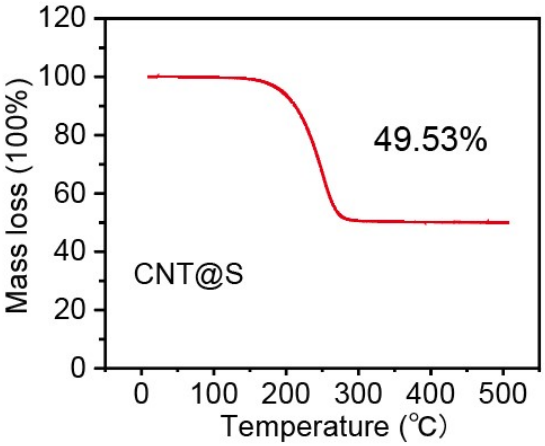

Fig. S5 TG curve of S@CNT.

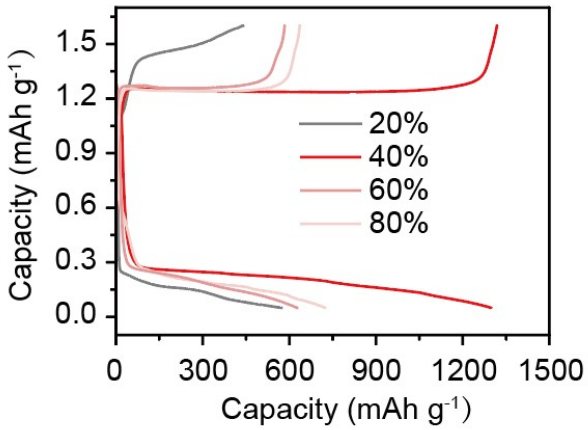

Fig. S6 Comparison of GCD curves of AZSBs using different volume content of ID.

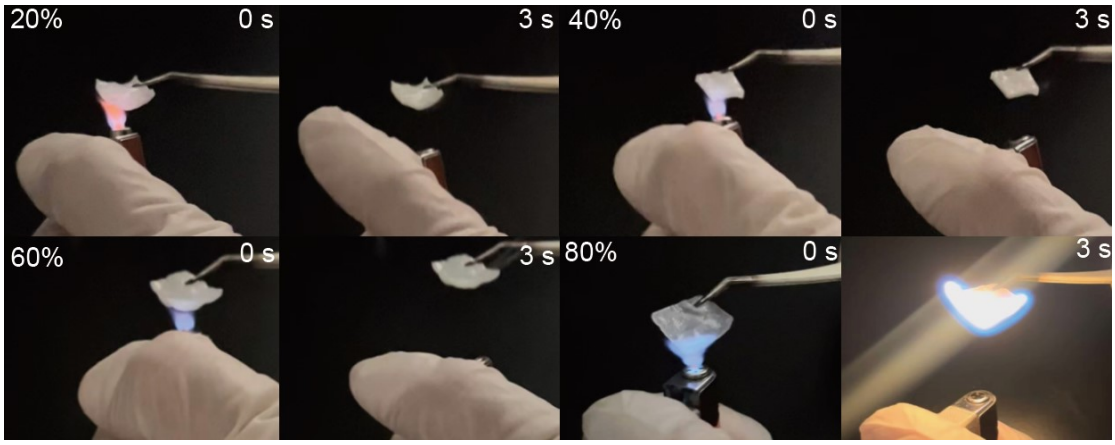

Fig. S7 Flammability test of IDW electrolytes with different ID concentrations.

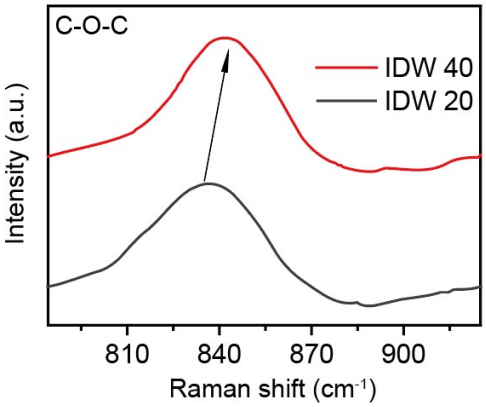

Fig. S8 Raman spectra of IDW with ID volume contents of 40% and 20%.

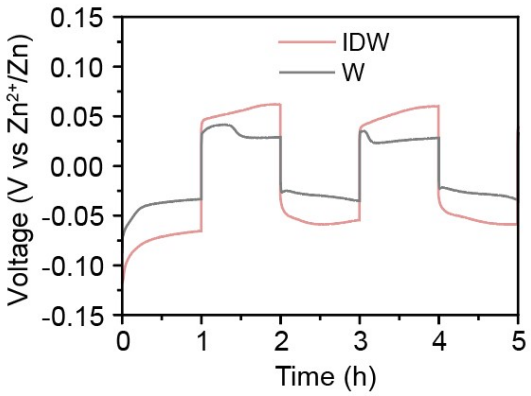

Fig. S9 Comparison of overpotential for nucleation between two types of electrolytes using Zn||Zn symmetric cells.

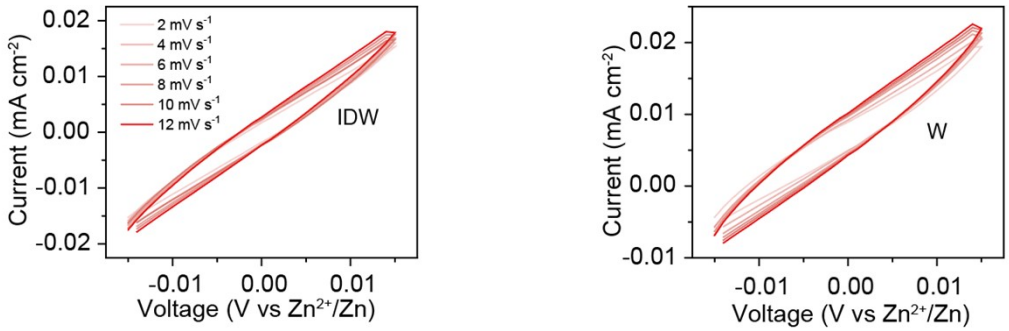

Fig. S10 Cyclic voltammogram curves of Zn||Zn symmetric cells using IDW and W electrolytes within a voltage range from −15 mV to 15 mV under various scanning rates.

Notes. EDLC at the Zn anode using W and IDW as electrolytes was measured by CV in the non-Faradic voltage range The EDLC is calculated through the equation of $C = i_c/v$, where C is the capacitance, i_c is the double layer current ($i_c = (i_{0v+} - i_{0v-})/2$), v is the scan rate. The linear dependence of the i_c on v can be used to determine the capacitance. C can be obtained from the slope of the i_c versus v graphs.

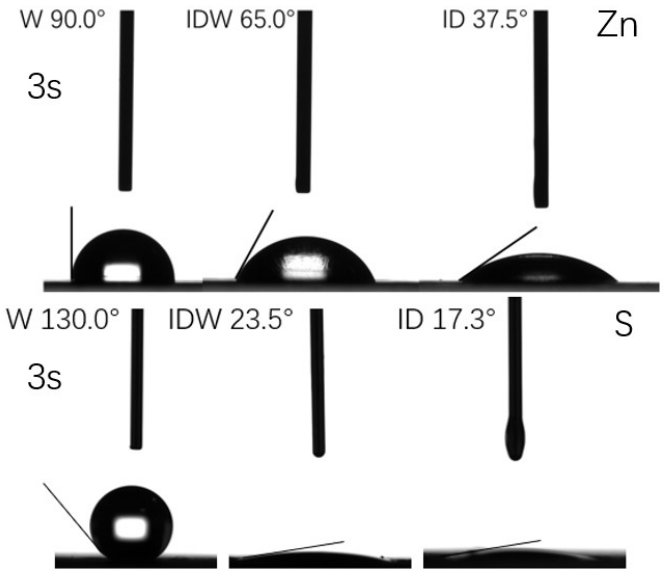

Fig. S11 Contact angle images of W, ID and IDW on zinc anodes and S cathode

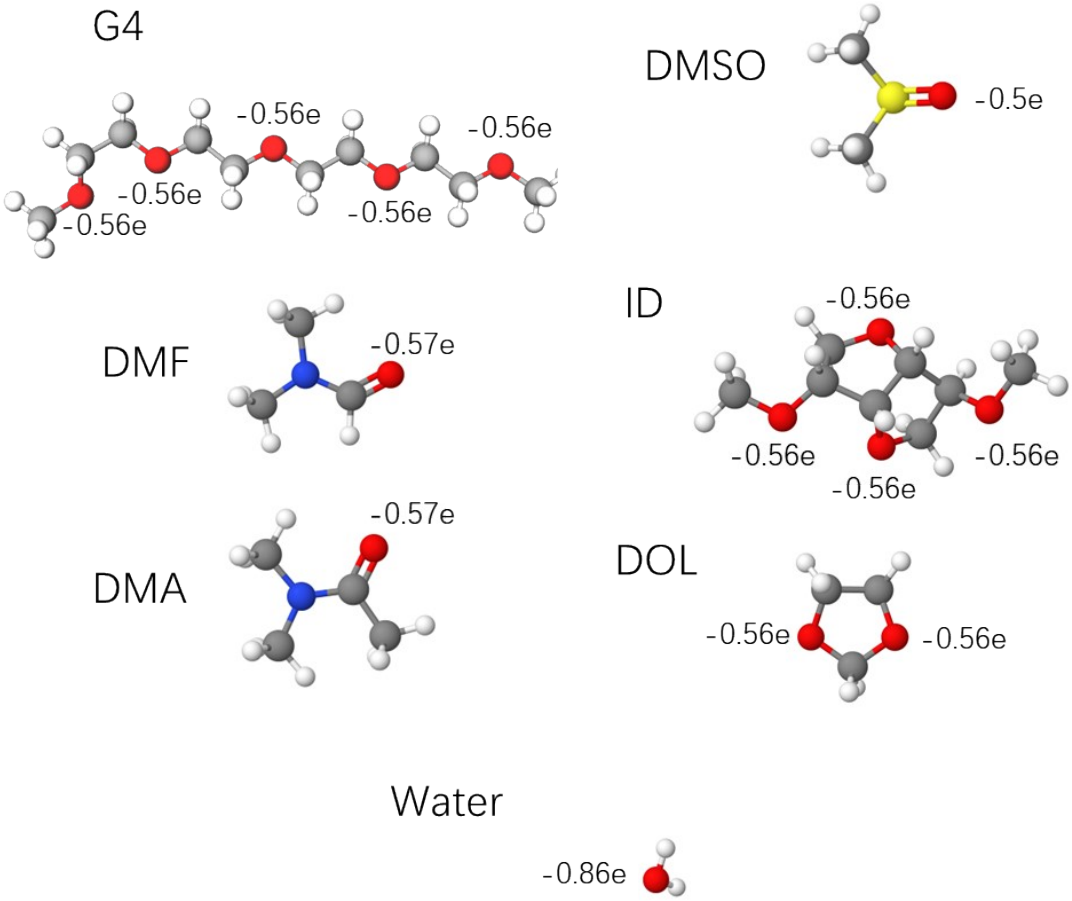

Fig. S12 Ball-and-stick models of the G4, DMF, DMA, DMSO, ID, DOL, and water with corresponding electron charges of oxygen atoms.

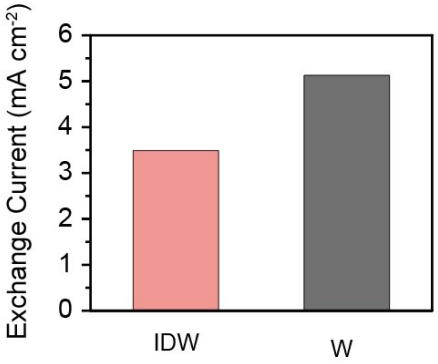

Fig. S13 The $j_{0,app}$ obtained from nucleation overpotential at different current densities.

Notes. The calculated exchange current density (j_0) can be termed as an "apparent" kinetic descriptor. The calculation and derivation of the apparent exchange current density ($j_{0,app}$) in this work are primarily based on methodologies established in recently reported literature (Phys. Chem. Chem. Phys., 2002, 4, 1067-1071; Energy Environ. Sci., 2025, 18, 2599-2609). Based on the Butler-Volmer equation in electrochemical kinetics, the relationship between overpotential and current density under high overpotential follows the Tafel equation:

$$\eta = \frac{RT}{aF}\ln\frac{j}{j_{0,app}} \quad (3)$$

Where η is the overpotential, j is the current density (mA cm^{-2}), $j_{0,app}$ is the exchange current density (mA cm^{-2}), α is the charge transfer coefficient, F is the Faraday constant (96485 C mol^{-1}), R is the gas constant (8.314 J mol^{-1} K^{-1}), and T represents the temperature (298.15 K). When nucleation occurs, the corresponding overpotential is referred as the nucleation overpotential η, and the corresponding current density is denoted as j. Substituting η and j into the Tafel equation yields:

$$j_{0,app} = j\exp\left(-\frac{aF\eta}{RT}\right) \quad (4)$$

Thus, by experimentally measuring the nucleation overpotential η and the corresponding current density j and with knowledge of the charge transfer coefficient α, the exchange current density $j_{0,app}$ can be calculated.

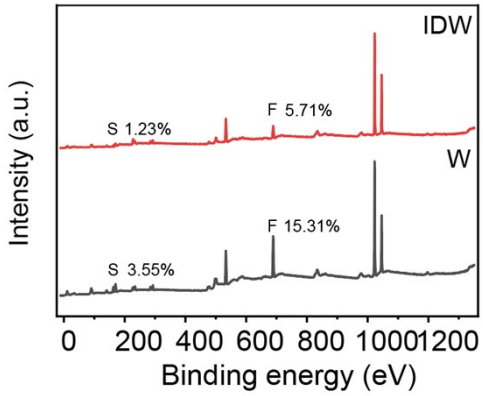

Fig. S14 The XPS survey spectra at the zinc anodes using IDW and W as electrolytes after cycling.

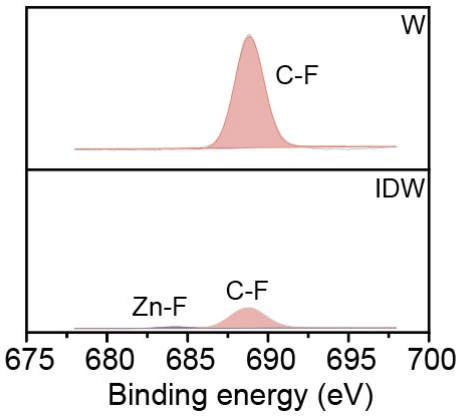

Fig. S15 The high resolution F 1s XPS spectra at the zinc anodes using IDW and W as electrolytes after cycling.

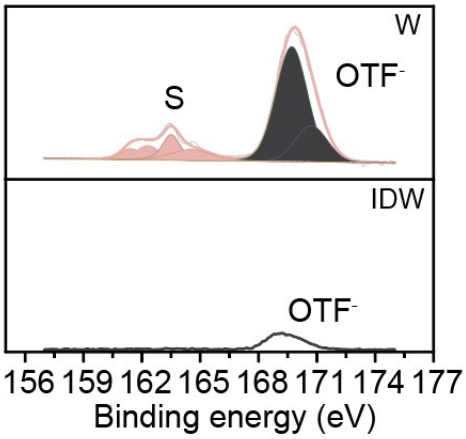

Fig. S16 The high resolution S2p XPS spectra at the zinc anodes using IDW and W as electrolytes after cycling.

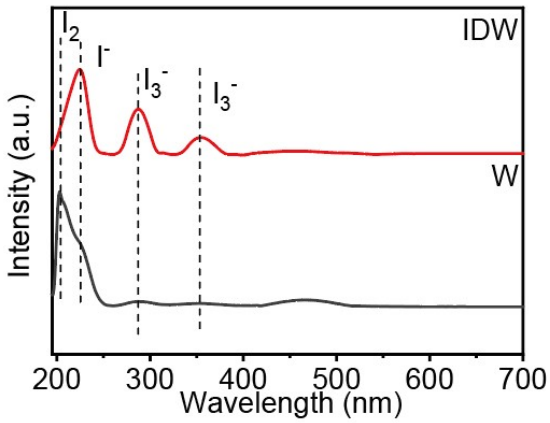

Fig. S17 UV–vis spectroscopy using IDW and W as electrolytes after cycling.

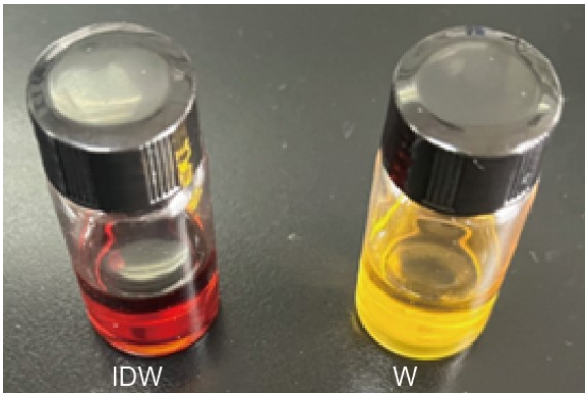

Fig. S18 Optical images of the two types of electrolytes.

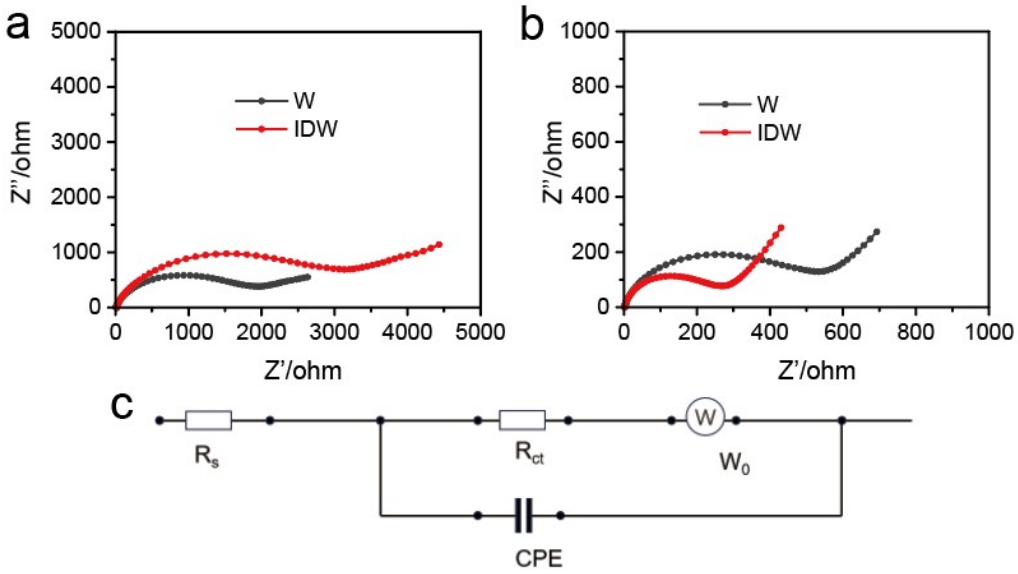

Fig. S19 Nyquist spectrum of ZSBs operated using IDW and W as electrolytes at fresh state (a) and after 30 th cycle (b). (c) Corresponding equivalent circuit diagram

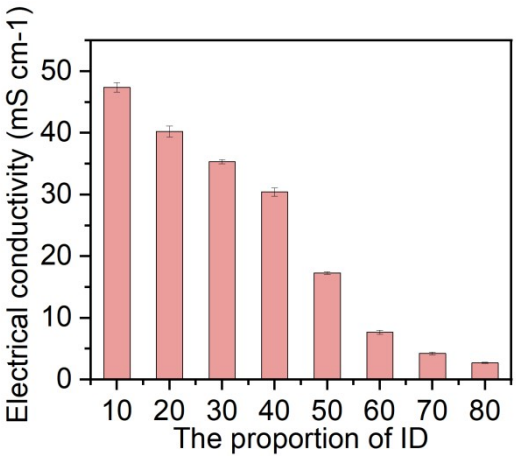

Fig. S20 Ionic conductivities of ID (n %) W electrolyte with different ID contents.

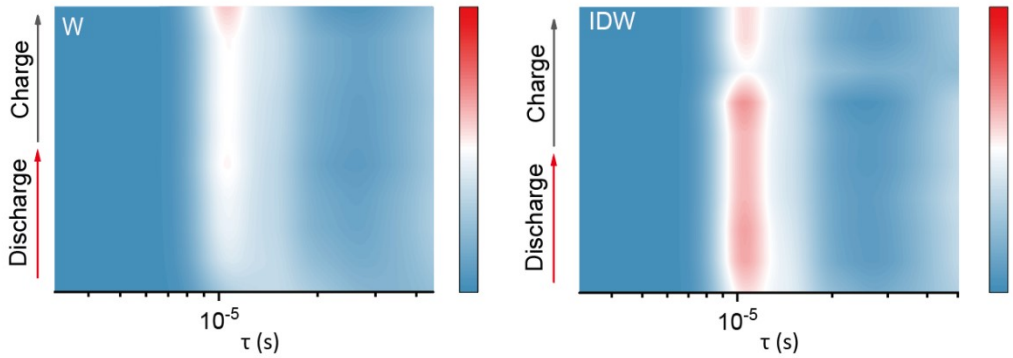

Fig. S21 Corresponding *in-situ* relaxation time distribution of IDW- and W- based batteries.

Table S1 The sulfur carbon analyzer analyzes the content of S in S@CNT.

Test quality(g)	C(wt%)	S(wt%)
0.0171	/	49.31

Table S2 The physicochemical properties of IDW with different ID volume contents.

	Electrical conductivity (mS cm^{-1})	Viscosity (mPa.s)	R_{ct} (Ω)	Migration number
IDW 20	44.1	25.31	1953.0	0.45
IDW 40	37.3	31.55	2371.0	0.37
IDW 60	17.3	45.92	3007.0	0.25
IDW 80	10.7	51.23	3713.0	0.21

Table S3 Comparison of AZSBs battery report employing IDW and W as electrolytes.

Electrolyte	**S loading** (mg cm^{-2})	**E/S** (μL mg^{-1})	**N/P**	**E. V./cell** (μL)	**Areal capacity** (mAh cm^{-2})	**CE**	**OCP** (V)	**Voltage window** (V)	**Energy density** (Wh kg^{-1})
IDW	1.5	17.4	4.93	40	2.37	~99%	1.25	0.05-1.6	426.3
W	1.5	17.4	6.96	40	1.68	~93%	1.23	0.05-1.6	237.7

Notes. Sulfur loading mass at the cathode: The total sulfur mass loaded on the cathode was measured to be 2.3 mg by averaging three cathode plates. The cathode current collector had a diameter of 14 mm, corresponding to a geometric area of 1.53 cm^2. Based on these values, the areal sulfur loading was calculated to be 1.5 mg cm^{-2}.

The electrolyte dosage was 40 μL, yielding an E/S ratio (electrolyte-to-sulfur ratio) of 40 / 2.3 = 17.4 μL mg^{-1}.

The N/P ratio is defined as the areal capacity of the anode divided by the areal capacity of the cathode. The calculation of the theoretical areal capacity of the anode: A Zn foil with a thickness of 20 μm was employed in this work. Given the theoretical specific capacity of Zn is 820.0 mAh g^{-1} and the density of Zn is 7.14 g cm^{-3}, the theoretical volumetric capacity is calculated as 5850 mAh cm^{-3}. The resulting areal capacity is therefore: 0.002 cm × 5850 mAh cm^{-3} ≈ 11.7 mAh cm^{-2}. With the known areal capacity of the cathode being 2.37 mAh cm^{-2} for IDW-based AZSB and 1.68 mAh cm^{-2} for W-based AZSB, the corresponding N/P ratios are calculated to be 4.93 and 6.96, respectively.

Table S4 Comparison of electrolyte systems and key performance metrics in recently reported AZSBs.

Electrolyte	Initial capacity (mAh g^{-1})	Cycling Stability	Initial CE	Refs.
2 M $Zn(OTf)_2$ + ID + 0.15 wt.% I_2	1573 @0.1 A g^{-1}	70% @2 A g^{-1} (250 cycles)	~100%	This work
1 M $Zn(CH_3COO)_2$ + 0.05 wt.% I_2	1105 @0.1 A g^{-1}	85% @1 A g^{-1} (50 cycles)	＞100%	[3]
1 M $ZnCl_2$ + D-Zn-Li 5% AN	846 @0.5 A g^{-1}	21% @1 A g^{-1} (400 cycles)	~100%	[4]
$Zn(CH_3COO)_2$-I_2/W-EG	511 @1 A g^{-1}	39.7% @1 A g^{-1} (500 cycles)	~100%	[5]
2 M $Zn(OTf)_2$ + 40% (vol)Tetraglyme + 0.15 wt.% I_2	1140 @0.5 A g^{-1}	70% @4 A g^{-1} (600 cycles)	~100%	[6]
1 M $Zn(OTf)_2$+DMC + I_2	1167 @0.1 A g^{-1}	47.6% @1 A g^{-1} (200 cycles)	~100%	[7]
3 M $ZnSO_4$ + 1 wt.% iodinated thiourea (TUI)	1410 @0.1 A g^{-1}	71% @2 A g^{-1} (300 cycles)	~100%	[8]
3 M $Zn(OTf)_2$+ACN+I_2	607 @0.2 A g^{-1}	71% @0.1 A g^{-1} (25 cycles)	79.8%	[9]
3M $Zn(OTf)_2$+I_2	788 @0.2 A g^{-1}	33% @2 A g^{-1} (50 cycles)	~100%	[10]
3M $Zn(OTf)_2$	768 @0.1 A g^{-1}	~	~	[11]
1 M $Zn(CH_3COO)_2$+PEG 400	1116@0.1 A g^{-1}	~	~	[12]

Notes and references

1. C. Johans, P. Liljeroth and K. Kontturi, Phys. Chem. Chem. Phys., 2002, 4, 1067–1071.
2. E. J. F. Dickinson and A. J. Wain, J. Electroanal. Chem., 2020, 872, 114145.
3. W. Li, K. Wang and K. Jiang, *Adv. Sci.*, 2020, **7**, 2000761.
4. M. Cui, J. Fei, F. Mo, H. Lei and Y. Huang, *ACS Appl. Mater. Interfaces*, 2021, **13**, 54981-54989.

5. Amiri, R. Sellers, M. Naraghi and A. A. Polycarpou, *ACS Nano*, 2023, **17**, 1217-1228.
6. M. Yang, Z. Yan, J. Xiao, W. Xin, L. Zhang, H. Peng, Y. Geng, J. Li, Y. Wang, L. Liu and Z. Zhu, *Angew. Chem. Int. Ed.*, 2022, **61**, e202212666.
7. D. Patel, A. Dharmesh, Y. Sharma, P. Rani and A. K. Sharma, *Chem. Eng. J.*, 2024, **479**, 147722.
8. D. Liu, B. He, Y. Zhong, J. Chen, L. Yuan, Z. Li and Y. Huang, *Nano Energy*, 2022, **101**, 107474.
9. Z. Ge, H. Liu, S. Wang, Y. Ma, W. Xu, L. Su, L. Han, L. Gong and J. Wang, *ChemSusChem*, 2025, **18**, e202401429.
10. Z. Xu, Y. Zhang, W. Gou, M. Liu, Y. Sun, X. Han, W. Sun and C. Li, *Chem. Commun.*, 2022, **58**, 8145-8148.
11. D. Patel and A. K. Sharma, *Energy Fuel.*, 2023, **37**, 10897-10914.
12. T. Zhou, H. Wan, M. Liu, Q. Wu, Z. Fan and Y. Zhu, *Mater. Today Energy*, 2022, **27**, 101025.
13. C. Johans, P. Liljeroth and K. Kontturi, Phys. Chem. Chem. Phys., 2002, **4**, 1067-1071.
14. S. Li, Y. Zhong, J. Huang, G. Lai, L. Li, L. Jiang, X. Xu, B. Lu, Y. Liu and J. Zhou, Energy & Environ. Sci., 2025, **18**, 2599-2609.